Biosensors and Bioelectronics 141 (2019) 111337

Contents lists available at ScienceDirect

Biosensors and Bioelectronics

journal homepage: www.elsevier.com/locate/bios

Label free phosphate functionalized semiconducting polymer dots for detection of iron(III) and cytochrome c with application to apoptosis imaging

Mojtaba Shamsipur[a,*], Ammar Chabok[b,1], Fatemeh Molaabasi[c,1], Amir Seyfoori[c], Behnam Hajipour-Verdom[d], Behnaz Shojaedin-Givi[e], Mosslim Sedghi[d], Hosein Naderi-Manesh[d], Ali Yeganeh-Faal[f]

[a] Department of Chemistry, Razi University, Kermanshah, Iran
[b] Department of Chemistry, Faculty of Basic Sciences, Tarbiat Modares University, Tehran, 14115-154, Iran
[c] Department of Biomaterials and Tissue Engineering, Breast Cancer Research Center, Motamed Cancer Institute, ACECR, Tehran, Iran
[d] Department of Biophysics, Faculty of Biological Sciences, Tarbiat Modarres University, Tehran, 14115-154, Iran
[e] Department of Nanobiotechnology, Faculty of Biological Sciences, Tarbiat Modares University, Tehran, 14115-154, Iran
[f] Department of Chemistry, Faculty of Basic Sciences, Payame Noor University, Tehran, Iran

ARTICLE INFO

Keywords:
Phosphate-functionalized polymer dots
Fluorescent nanoprobe
Apoptosis imaging
Fe(III)
Cytochrome c

ABSTRACT

We report on facile synthesis and characterization of phosphate-functionalized polymer dots (PDs) by doping tributyl phosphate (TBP) in a semiconducting polymer poly[9,9-dioctylfluorenyl-2,7-diyl)-co-1,4-benzo-{2,10-3}-thiadiazole)] (PFBT). Then, the prepared TBP@PFBT PDs were used to develop a very high sensitive probe for detection Fe^{3+}, Cu^{2+} ions and Cytochrome c based on aggregation induced fluorescence off mechanism. The PDs exhibited a linear dynamic range for Fe^{3+} from 0.1 to 2 nM with a detection limit of 30 pM and for Cu^{2+} from 2.0 to 50.0 nM with a detection limit of 0.35 nM. Meanwhile, this probe showed a linear dynamic range for Cyt c from 175 to 1750 pM with a detection limit of 32.7 pM. The TBP@PFBT PDs is a simple, one-step, fast, non-invasive, label-free, and inexpensive probe that is capable of online apoptosis monitoring response to drugs with an ever-present opportunity to contribute in a variety of in-vitro and in-vivo biological applications. We also obtained sharp, specific 2D and 3D imaging results for early stage apoptosis in breast cancer cells. Moreover, this technique possesses the advantage of rapid determination of Fe^{3+} ion in biological or environmental samples. Importantly, this label-free assay provides short determination time of only a few min, easy operation and very low LOD allowing 100–4000 times increased in sensitivity over previously reported probes, together with high selectivity without need to using biorecognition elements like enzymes, antibodys and/or aptamers. Such excellent features make the TBP@PFBT PDs an excellent probe for successful apoptosis imaging in live cells.

1. Introduction

Iron and copper are two essential metals in manycrucial biological functions of cells. Because these two metals are used extensively in agriculture and industry, a trace amount of their ions may exist in natural waters. The free Fe^{3+} and Cu^{2+} ions are known to induce cytotoxicity that causing serious problems such as liver and kidney disease and even death (Georgopoulos et al., 2001; Kozlowski et al., 2006; Ryan and Ray, 2004; Torrado et al., 1998). Also, it is great motivators to develop very high sensitive approaches to analysis metals in a range of ppb or lower in some industries as measuring trace contamination in semiconductor-grade silicon (Fabry et al., 1994). Analysis methods at this levelneed expensive instrumentation and time-consuming routs and as a result, there is a great effort to develop, simple and easy methods based on cheap instrumentation.

Apoptosis is a crucial programmed cell death, which refers to pathways that regulated cellular homeostasis and finally lead the cells to differentiation or death(Sun et al., 2010). Apoptosiscan interestingly track various biological processes including pathogenesis of different malignancies and autoimmune diseases, anticancer drug screening, normal cell turnover and etc.(Ruan et al., 2012) Generally, apoptosis can be followed by a change in cell morphology, mitochondrial function

* Corresponding author.
E-mail address: mshamsipur@yahoo.com (M. Shamsipur).
[1] These authors have the same contributions in this work.

https://doi.org/10.1016/j.bios.2019.111337
Received 14 January 2019; Received in revised form 6 May 2019; Accepted 17 May 2019
Available online 20 May 2019
0956-5663/

and caspase activity, as well as protein release from the cell, surface lipid translocation, redox state shift, and DNA condensation/fragmentation (Ruan et al., 2012; Wu et al., 2012). These processes might be assayed by several approaches as microscopic imaging, flow cytometry, terminal deoxynucleotidyl transferase-mediated dUTP nick end-labeling (TUNEL assay), single-cell gel electrophoresis (Comet assay), mitochondrial membrane potential analysis, and Western blotting analysis (Subarkhan et al., 2018; Sun et al., 2010; Wu et al., 2012). These methods not only are qualitative invasive assessments, but also perform under rigorous conditions, together with various manipulations and costly equipment(Hsu et al., 2018; Tong et al., 2014). In this way, there are also some limitations in relation to FITC Annexin V and propidium iodide (PI) dye-mediated apoptosis imaging, due to their nonspecific binding to negatively charged phosphatidylserine (PS) present on the apoptotic cell membrane and other biological situations like myotube formation and necrosis, as well as in relation to TUNEL assay of apoptotic DNA fragmentation because of the presence of many reaction steps and internucleosomal breaks associated with other biological process except apoptosis (Ruan et al., 2012; Sun et al., 2010). Cytc is considered as an effective biomarker for early-stage cell apoptosis assay, which releases through mitochondrial membrane permeabilization mediated during intrinsic apoptotic pathway (Song et al., 2004,Torkzadeh-Mahani et al., 2012, Waterhouse and Trapani, 2003; Wen et al., 2014, Zhang et al. 2012).

In recent years, the development of a simple, fast and specific approach to identification and quantification of early-stage of apoptosis and/or apoptosis imaging has become an area of focused interest. One of the best ways to investigate this issue is to design apoptosis sensors based on biocompatible and highly fluorescent nanomaterials. Among different fluorescent probes, semiconducting conjugated polymer dots (PDs) are well-known as highly fluorescent nanomaterials with small size, excellent brightness, good photo-stability, fast radiative rates and easy to synthesis and to surface modification (Wu and Chiu, 2013; Wu et al., 2010). In fact, PDs exhibit a wide variety of optoelectronic and biological applications such as light-emitting diodes, photovoltaic devices, high-resolution single particle tracking, biochemical sensors, drug delivery, photodynamic therapy, and in vitro and in vivo imaging (Chabok et al., 2019; Li et al., 2014; Nasirian et al., 2017; Sun et al., 2013; Wu and Chiu, 2013; Wu et al. 2008a, 2010, 2014). PDs possess greater brightness and have more resistant to photo bleaching as well as larger optical cross sections even in red wavelength region, allowing the best tissue penetration of light and are biocompatible nanomaterials in various cellular assays, compared to organic fluorophores, green fluorescent proteins (GFPs) and quantum dots (QDs) (Sun et al., 2013; Wu and Chiu, 2013; Wu et al. 2010, 2014).

In this work, we have designed novel phosphate functionalized polymer dots by doping tributyl phosphate (TBP) in a semiconducting polymer poly[9,9-dioctylfluorenyl-2,7-diyl)-co-1,4-benzo-{2,10-3}-thiadiazole) (PFBT) to form TBP@PFBT PDs. Here, folding of the hydrophobic polymer chains provide a hydrophobic platform in which the butyl groups as hydrophobic moiety of TBP anchor inside of the hydrophobic matrix of polymer dot core, while the phosphate group as a hydrophilic moiety is exposed at the surface of PDs in contact with aqueous solution. TBP is an interesting complexing agent, which forms a hydrophobic complex with some metals and is widely used in the solvent-solvent extraction of leached metals from ores in the nuclear industry (Benedict et al., 1981). In TBP@PFBT PDs, thephosphate moiety serves as an active chelating group for metal ions without any other modification. The probe showed high sensitivity toward Fe^{3+}, Cu^{2+} and Cyt c with fast response, upon an aggregation induced fluorescence off mechanism, as proved by transmission electron microscopy (TEM), dynamic light scattering (DLS) and UV–Vis spectroscopy. The probe was successfully applied to sensitive determination of iron(III) in environmental samples and to detection of Cyt c in cell lyses and apoptosis imaging of live cells. It was showed that the nanoprobes are capable of 2D and 3D imaging of apoptosis in developed breast tumor models, so that it can emulate the real in-vivo tumor micro environment condition, as a micro spheroid comprising extracellular matrix.

2. Experimental section

2.1. Reagents and apparatus

Reagent grade poly[(9,9-dioctylfluorenyl-2,7-diyl)-alt-co-(1,4-benzo-(2,1',3)-thiadiazole)] (PFBT, 10 kDa MW, polydispersity index (PDI) of 2.3 and cytochrome c (Cyt c) (both from Sigma Aldrich), tributhylphosphate (TBP), NaH_2PO_4, Na_2HPO_4, Li_2SO_4, KCl, NaCl, NaOH, $BaCl_2$, $CaCl_2$, $FeCl_2$, $HgCl_2$, $MgCl_2$, $MnCl_2$, $NiCl_2$, $SnCl_2$, $SrCl_2$, $ZrOCl_2$, $AgNO_3$, $AlCl_3$, $Co(NO_3)_2$, $Cu(NO_3)_2$, $Cd(NO_3)_2$, $Pb(NO_3)_2$, $Zn(NO_3)_2$, $FeCl_3$, $Ce(NO_3)_3$, $Cr(NO_3)_3$, sodium phthalate(all from Merck) were of analytical grade and used without further purification.

Spectrofluorimetric measurements were performed using an Agilent Cary Eclipse fluorescence spectrometer (Agilent Technologies, US). The emission spectra were recorded over the wavelength range of 470–700 nm, upon excitation at 460 nm, at a scan rate of 1500 nm min^{-1}. Both the excitation and emission spectral band pass were set at 10 nm. The UV–Vis absorption spectra were recorded on a model Shimadzu UV 2550 (Shimadzu, Japan). The transmission electron microscopy (TEM) images were recorded on an EM-10C Zeiss transmission electron microscope (Zeiss, Germany) with an accelerating voltageof 150 kV. Zeta potential and dynamic light scattering (DLS) were measured using a Zetasizer Nano ZS instrument (Malvern Instruments Ltd., UK). Atomic absorption spectroscopy measurements were carried out by a PerkinElmer AAnalyst 100 spectrometer. Fluorescence imagingswere recorded on an Olympus fluorescence microscope equipped with a blue filter (480 nm excitation, > 500 nm emission) for detection of TBP@PFBT and a green filter (520 nm excitation, > 600 nm emission) for DOX detection under ambient conditions.

2.2. Synthesis, characterization and application of phosphate functionalized PDs

Phosphate functionalized PDs were synthesized by a nanoprecipitation technique (Wu and Chiu, 2013; Feng et al., 2013). Briefly, 1 $mgmL^{-1}$solutions of PFBT and TBP in THF were prepared as the stock solutions. Then, 250 μL of dissolved PFBT and 50 μL of dissolved TBP added to 5 mL THF and mixed well. After that, the resultant mixture injected immediately to 10 mL of distilled water under sonication and remained 2 min under sonication. Then, THF was removed by N_2 bubbling on a 70 °C hotplate followed by filtration through a 0.2 μm filter. The synthesized PDs were then characterized by TEM, and DLS.

For the determination of Fe^{3+} in tap water, 25 μL of synthesized TBP@PFBT polymer dots solution was added into 2 mL pure water in a fluorescence cuvette in the excess amount of EDTA (to remove other metal ions interference) as blank sample. Then 20 μL of tap water was spiked to the cell and the fluorescence intensity decrease was recorded. For determination of Cyt c in cell lyses MCF-7 and HFF cells treated with DOX after 0, 6 h, 12 h and 24 h, 25 μL of TBP@PFBT polymer dots solution was added into 2 mL pure water in a fluorescence cuvette as blank sample. Then 2 μL of cell lyses was spiked to the cell and the fluorescence intensity decrease was recorded. Then different amount of Cyt c spiked to the cuvette and fluorescence spectra were recorded.

2.3. Cell culture and spheroid formation

Thehuman breast adenocarcinoma cell line (MCF-7) and human foreskin fibroblast (HFF) cells used in this current study were obtained from the National Cell Bank of Iran (NCBI) located in Pasteur Institute of Iran (IPI). The cells were allowed to grow in Dulbecco's Modified Eagle's Medium (DMEM) in neutral pH (7.2–7.4), which supplemented

with 10% (v/v) heat-inactivated (50 °C, 30 min) from Fetal Bovine Serum (FBS), 2 mM L-glutamine, 100 unitsmL^{-1} of penicillin and 100 mgmL^{-1} of streptomycin at 37 °C and 5% CO_2 in a humidified incubator. Then, the cells were trypsinized (0.025% trypsin, 0.02% EDTA) after they were grown until 70–80% confluent. Prior to treatments, the cells were allowed overnight to reattach to the bottom of cell culture plate.

To investigate the effect of 3-dimensional cell gathering on the fluorescent intensity of the cancer cells, before and after chemotherapeutic drug treatment, the semi-micro-tumor tissue made of MCF-7 cell spheroids wereprepared. To generate MCF-7 tumor spheroids, non-cell adherent conical agarose substrate was used to stimulate spheroid formation instead of monolayer proliferation. In this way, the agarose platforms were firstly soaked in the culture media and the prepared cell suspension with the densities of 500×10^3 cell were loaded on it. The cell loaded agarose substrate was kept in incubator for 4 days to form the spheroid (Seyfoori et al., 2018).

The TBP@PFBT PDs solution asmonolayer cell culturing platform was added to the growth medium at 5 μLmL^{-1} (0.5% final) and then was applied to the top of the spheroids in the agarose platform, followed by 2 h incubation to let fully diffuse in the 3D structure of the tumor spheroids. Apoptosis induction was also performed and investigated using Dox as a model drug at different concentrations and treatment timeon day 7 of storage. Fluorescent imaging was conducted afterwards followed by triple washing of the spheroids to eliminate extra PDs illumination and, subsequently,the background noises.

3. Results and discussion

3.1. Characterization and optical properties of synthesized TBP@PFBT PDs

PDs were prepared by the nano-precipitation technique, in which the rapid mixing of THF solution of polymers with water resulted in dot formation, driven by hydrophobic interactions (Feng et al., 2013, Wu et al., 2011). The synthesized PDs were then characterized by TEM and DLS and the results are shown in Fig. 1A. The TEM image reveals that the TBP@PFBT PDsare roughly spherical shape with an average diameter of about 20 nm; this result was further confirmed by DLS analysis shown in Fig. 1B.

To further study the optical properties of the PDs, their UV–Vis absorption and PL spectra were obtained at room temperature and the results are shown in Fig. 1D. As seen, the PDs show a broad absorption band ranging from 300 to 520 nm that is suitable for laser excitation and fluorescence microscopy. The PDs possess a strong yellow emission centered at 540 nm when it was excited at a wavelength of 460 nm. Additionally, the dispersion of PDs exhibited a strong yellow emission under UV lamp illumination (365 nm), as shown in inset of Fig. 1D.

3.2. Iron(III)- and copper(II)-induced PL quenching of TBP@PFBT PDs

While the bare PFBT PDs do not have selectivity to any analyte, their surface functionalization and/or doping of sensing molecules inside themcan make the polymer dotsselectively responsiveto traces of a variety of metal ions and biomolecules (Chabok et al., 2019; Chan et al., 2011; Childress et al., 2012; Wu and Chiu, 2013; Wu et al., 2008b). In this work we used TBP to anchor phosphate groups on the surface of PFBT PDs. As shown in Scheme 1, the fluorescence of TBP@PFBT PDs selectively quenched in the presence of Fe^{3+} and Cu^{2+} ions in water. The aggregation and quenching behavior is related to the chelating interaction of phosphate groups on the surface of PDs with Fe^{3+} and Cu^{2+} ions in water. Phosphate chelating ability of iron and copper ions has been previously reported (Smolin et al., 2017; Zhang et al., 2014) and also similar fluorescence aggregation-caused quenching (ACQ)was reported in some other analogue systems (Chan et al., 2011; Meng et al., 2010; Huang et al., 2007). The distribution coefficients of Cu^{2+} and Fe^{3+} between aqueous phase and TBP phase is 0.156 and 378, respectively, that shows much more affinity of TBP to Fe^{3+} ions (Irving and Edgington, 1959). To prove this phenomenon, the transmission electron microscopy (TEM) and dynamic light scattering (DLS) measurements were performed before and after addition of Fe^{3+} (see Fig. S1). These measurements revealed that the diameter of TBP@PFBT PDs was about 20 nm on average, but after aggregation by adding Fe^{3+} reached to a final diameter of about 400 nm. No sign of scattering was observed in UV/Vis spectrabefore and after the addition of Fe^3, suggesting the formation of small aggregates in presence of Fe^{3+} (Fig. S2). This data is consistent with TEM and DLS measurements.

We examined the performance of TBP@PFBT probe in a different buffer media and observed various behaviors of the probe towards Fe^{3+}

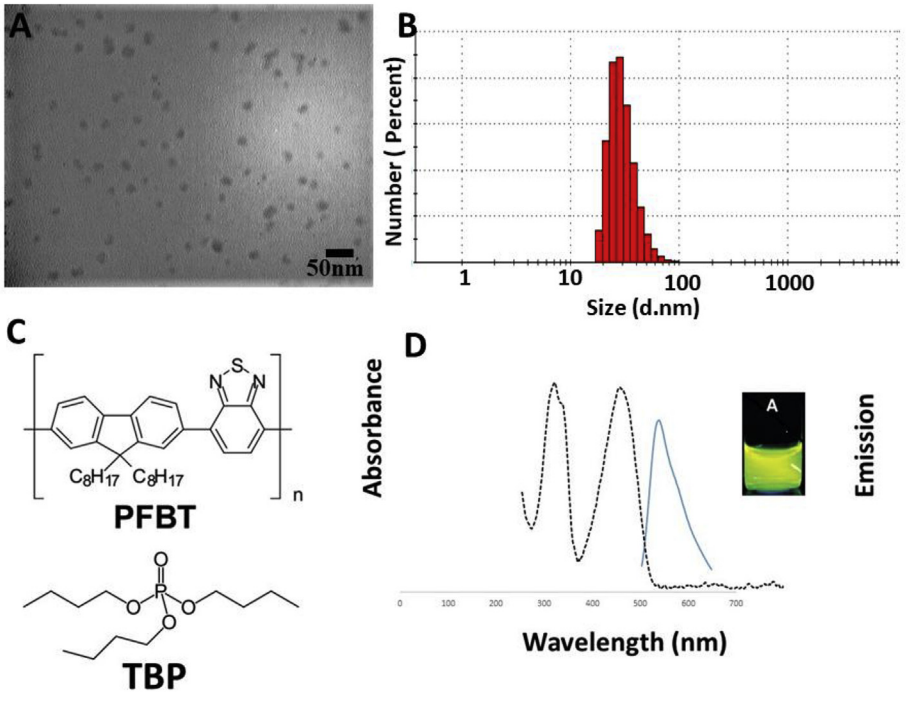

Fig. 1. (A)TEM and (B) DLS of TBP@PFBT PDs. (C)Chemical structures of PFBT and TBP and (D) The absorption and emission of TBP@PFBT PDs were shown in a dashed black line and a solid blue line, respectively. (For interpretation of the references to colour in this figure legend, the reader is referred to the Web version of this article.)

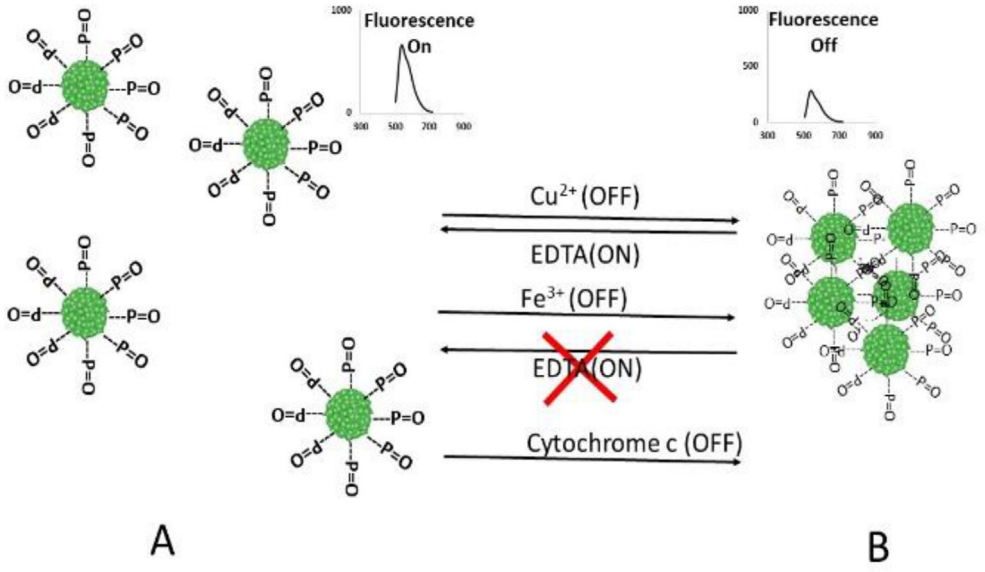

Scheme 1. Schematic illustration of sensing of Cu^{2+} and Fe^{3+} by TBP@PFBT PDs. (A). Aggregation induced fluorescence-off behavior of Fe^{3+} and/or Cu^{2+} and Cytochrome c. (B) While EDTA can reverse Cu^{2+} induced aggregation fluorescence-off, Fe^{3+} ion cannot be re-dispersed in the presence of EDTA.

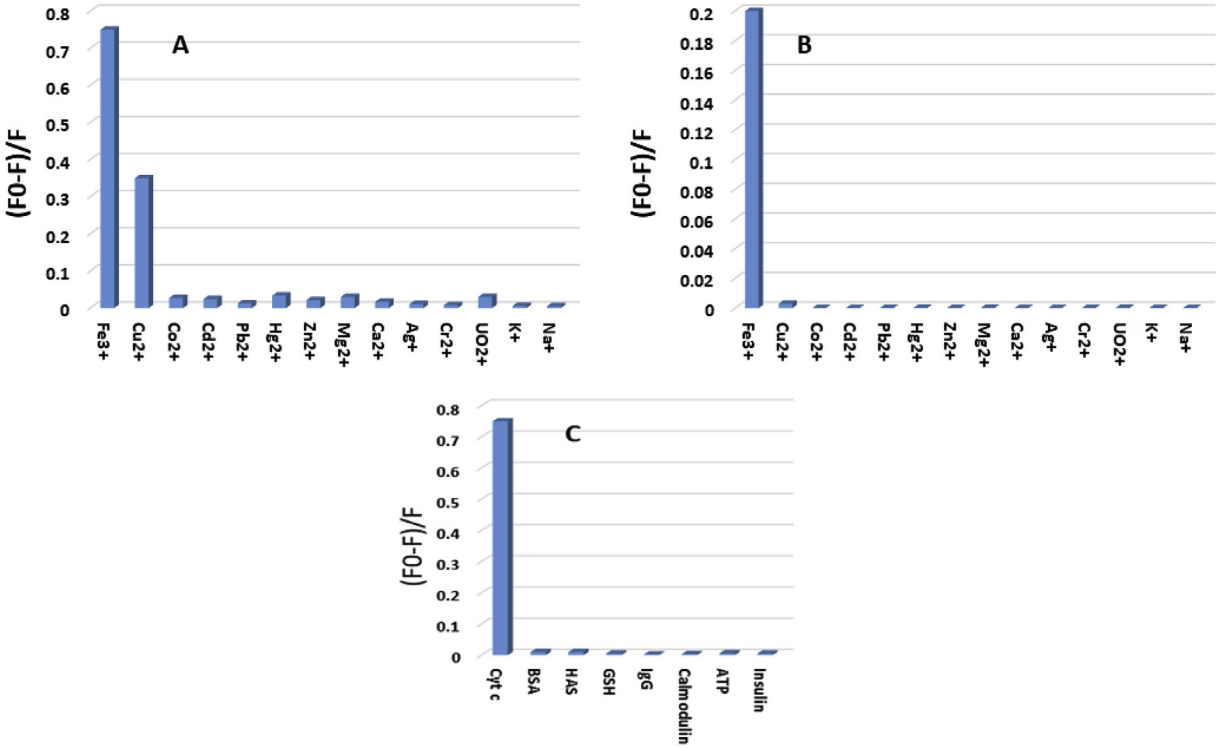

Fig. 2. (A) Selectivity of TBP@PFBT PDs toward 1 μM of different metal Ions in pure water. (B) Selectivity of PDs toward 2 nM (maximum linear range of Fe^{3+} detection) of different metal ions in pure water. (C) Selectivity of PDs toward 2 nM of different proteins.

and Cu^{2+} ions. At first, the selectivity of TBP@PFBT probe was investigated in pure water and found negligible fluorescence intensity changes in presence of other cations than the Fe^{3+} and Cu^{2+} ions (Fig. 2). However, the probe response in PBS solution is not fast and its response time differs depending on PBS concentration(e.g., less than 10 min in 2 mM of PBS and 15 min in 10 mM PBS). This may be due to similarity between PDs and TBP structures which both containing phosphate groups, enabling them to compete for the cation chelate formation. Meanwhile, in phthalate buffer, it was found that the TBP@PFBT probe is just sensitive to Fe^{3+} and does not have any response to Cu^{2+} ions. This can be described by the fact that phthalate is a strong complexing agent for Cu^{2+} ions, a binding constant much greater than that for phosphate groups of TBP on the surface of PDs with copper ions (Bartl and Kuppers, 1980). However, in the case of Fe^{3+} ions, phthalate could not overcome the very strong binding of the cation with the phosphate groups of TBP at the PDs surface.

Fig. 3A shows the emission spectra of TBP@PFBT PDs as a function of Cu^{2+} concentration. Fluorescence intensity decreased with increasing concentration of Cu^{2+} ions to a final concentration of 12 μM and after that the intensity remains almost constant, indicating that all phosphate groups of PDs have already been occupied by Cu^{2+} ions. Besides, the relative standard deviation (RSD) of the blank signal from

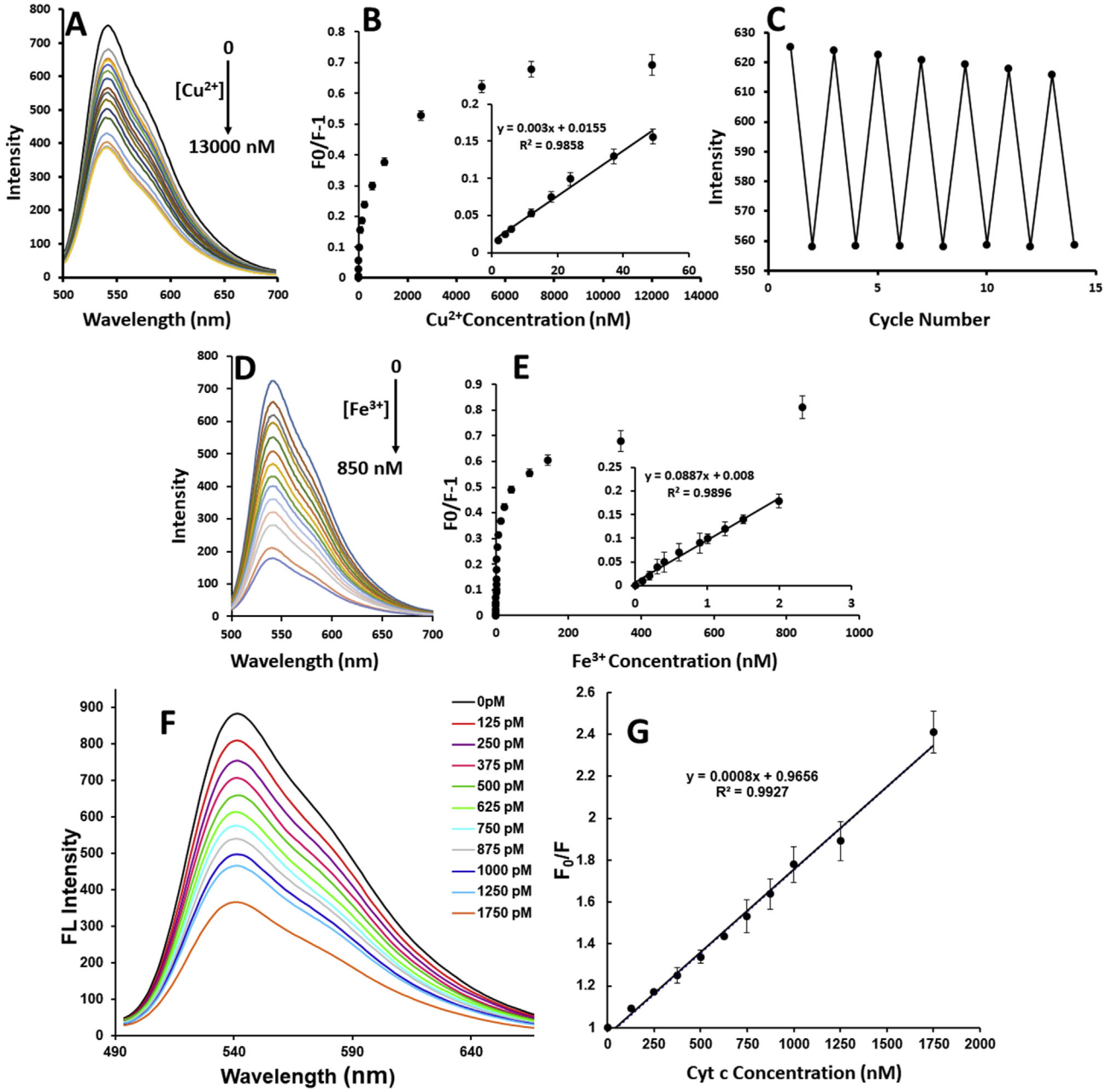

Fig. 3. (A) Fluorescence spectra of TBP@PFBT PDs in the presence of increasing Cu2+ concentration, from 0 to 13 μM. (B) A plot of fluorescence ratio as a function of Cu2+ concentration at λem of 540 nm. The inset shows a linear fit to the experimental points (R2 = 0.9858). (C) Cyclic fluorescence quenching and restoring after addition of Cu2+ and EDTA (50 nM), respectively. (D) Fluorescence spectra of TBP@PFBT PDs in the presence of increasing concentration of Fe3+ from 0 to 850 nM. (E) A plot of fluorescence ratio as a function of Fe3+ concentration at λem of 540 nm. The inset shows a linear fit to the experimental points (R2 = 0.9896). (F) Fluorescence spectra of TBP@PFBT PDs in the presence of increasing Cyt c concentration of Cyt c from 0 to 1750pM. (G) A linear plot of fluorescence ratio as a function of Cyt c concentration at λem of 540 nm. (R2 = 0.9927).

10 replicates was 1.2%. A good correlation coefficient (R^2 = 0.986) was obtained over the concentration range of 2.0–50.0 nM (Fig. 3B). The limit of detection (LOD) was calculated to be 0.35 nM, based on a signal to noise ratio of 3.0. The effect of ethylenediaminetetraacetic acid (EDTA) as a strong copper chelating agent, on re-dispersion of aggregated PDs was also studied and found that EDTA can almost fully restore the fluorescence intensity of PDs (Fig. 3C). The DLS experiments also confirmed the re-dispersion of aggregated PDs (Fig. S3). This process can be repeated many times without signal loss and also the aggregation and re-dispersion behavior of PDs completes in less than 1 min.

For Fe^{3+} ions, the dynamic linear range was from 0.1 to 2 nM, as shown in Fig. 3E,with a correlation coefficient of 0.99 and a LOD was 30 pM calculated based on a signal to noise ratio of 3. In Table S1are compared the figures of merit of some analytical methods and fluorescent probes for Fe^{3+}detection. Despite greater binding constant of EDTA toward Fe^{3+} (log K_f = 25.10) than Cu^{2+} (log K_f = 18.80), our findings revealed that the aggregated PDs by Fe^{3+} could not be recovered by EDTA even at high concentrations. This is most possibly due to much higher tendency of phosphate groups on the surface of TBP@PFBT PDs towards Fe^{3+} ion than the cation binding affinity to EDTA in aqueous solution. It should be noted that the distribution coefficients of Cu^{2+} and Fe^{3+} between aqueous phase and tributyl phosphate (TBP) phase are 0.156 and 378, respectively, that shows much higher affinity of TBP, as a model phosphate group at the surface of PDs, towards Fe^{3+} ions compared to Cu^{2+} (Irving and Edgington, 1959). In addition, the

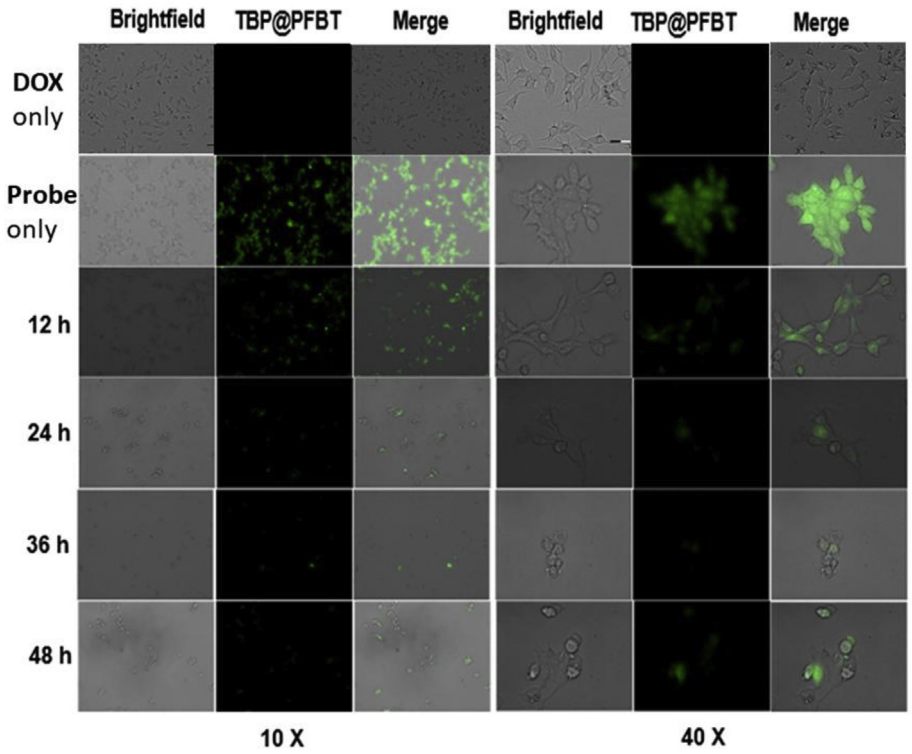

Fig. 4. Fluorescence responses of apoptosis in MCF7 cells incubated with 15 μg/mL TBP@PFBT probe for 1 h followed by a treatment of 4 μM DOX.

solution pH found to play an important role on the Fe^{3+}–EDTA chelation and the Fe^{3+} hydrolysis. The association constants for Fe^{3+}-EDTA chelates decreased between pH 7.0 and 9.0, mainly due to the formation of mixed EDTA-hydroxy chelates (Fe^{3+} $EDTA(OH)_2$) with more rapid dissociation kinetics. On the other hand, the solubility of Fe^{3+} is very low in neutral or alkaline pHs, due to formation of insoluble $Fe(OH)_3$ (Hudson et al., 1992; Sunda and Huntsman, 2003).

In order to demonstrate the application of this sensing system, we used tap water and mineral water samples to measure their iron content. Here, 20 μL of water samples was spiked to 2 mL of sample water in fluorescence cell to meet linear range of iron sensing (1000 times dilution). Then EDTA was added in excess amount to remove any Cu^{2+} interference and to accurately determine the Fe^{3+} ion content. The results obtained by this probe found to be in satisfactory agreements with those by atomic absorption spectrometry (AAS)(see Table S2). This finding demonstrated that TBP@PFBT PDs possess potential application highly selective and sensitive detection of iron ions in environmental samples. This probe is also applicable to copper measurement in samplescontaining no iron ions present.

3.3. Imaging of Cyt c and iron release for apoptotic studies

Since Cyt c contains heme groups consisting of a rigid porphyrin ring coordinated to a Fe^{3+} ion, we motivated to investigate its response to the TBP@PFBT PDs. Thus, the effect of concentration of Cyt c, as an early-stage apoptotic biomarker, on the emission spectra of TBP@PFBT PDs was studied. Although the semiconducting polymer dots are not toxic in general (Wu and Chiu, 2013), we further studied added the cytotoxicity of our probe and the results are shown in Fig. S5 in supporting information file, which clearly confirm the non-toxicity of the PDs prepared.

As it is seen from Fig. 3F and G, the fluorescence (FL) intensity was linearly decreased as a function of Cyt c concentration from zero to 1.75 nM (R^2 = 0.993), with a LOD of 32.7 ± 0.1 pM (S/N = 3). In pure water, the fluorescence quenching was fast and completed in less than 1 min, while in 10 mM PBS solution, maximum fluorescence quenching of TBP@PFBT PDs in the presence of 1 μM Cyt c was occurred in less than 15 min. Therefore, an appropriate time interval of 15 min was considered between the recorded spectra, to the desired calibration concentration. This idea further confirmed by evaluating of PDs specificity towards other interfering proteins including BSA, Lys, insulin, HAS, pepsin and trypsinand the results are shown in Fig. 2C. As seen, no significant changes were observed in FL intensity of TBP@PFBT for these non-iron binding proteins. Table S3 compares the analytical figures of merits of some analytical methods and fluorescent probes reported for Cyt c detection. As is quite obvious from Table S3, our PDs based sensor shows a significant improvement in detection limit over a variety of fluorescence, chemiluminescence, spectrophotometric, electrochemical and ICP-MS methods, previously reported in the literature, for detection of traces of Cyt c in real samples.

The excellent features of theTBP@PFBT PDs probe persuade us to apply it for apoptosis imaging in live cells. For this aim, human breast adenocarcinoma cell line (MCF7) and human foreskin fibroblast (HFF) cells were treated with 4 μMdoxorubicin (DOX) and cellular imaging was performed as a function of incubation times by an Olympus fluorescence microscope equipped with a blue filter (480 nm excitation, > 500 nm emission) for detection of TBP@PFBT and a green filter (520 nm excitation, > 600 nm emission) for DOX detection under ambient conditions. Upon incubation with TBP@PFBT, the MCF7 cells without DOX treatment showed strong green fluorescence signals, indicating retention mechanism, excellent cell permeability and endocytosis of probe and thus high PDs accumulation inside the cancer cells, especially, it seems that more diffuse fluorescent PDs (Fig. 4). However, the fluorescence of MCF7 cells gradually decreased with the apoptotic progressafter 12 h of DOX treatment, triggering the cytosolic release of Cytc into the cytoplasm as well as iron release. This was due toaggregation-caused quenching (ACQ) mechanism by which fluorescence signals of TBP@PFBT probe reaches a minimum almost at 24 h and after that remains constant during 24–48 h (Fig. 4). This could be ascribed in accordance with the previous findings related to complete release of Cytc during apoptosis (Akbari-Birgani et al., 2014; Shamsipur et al., 2016).

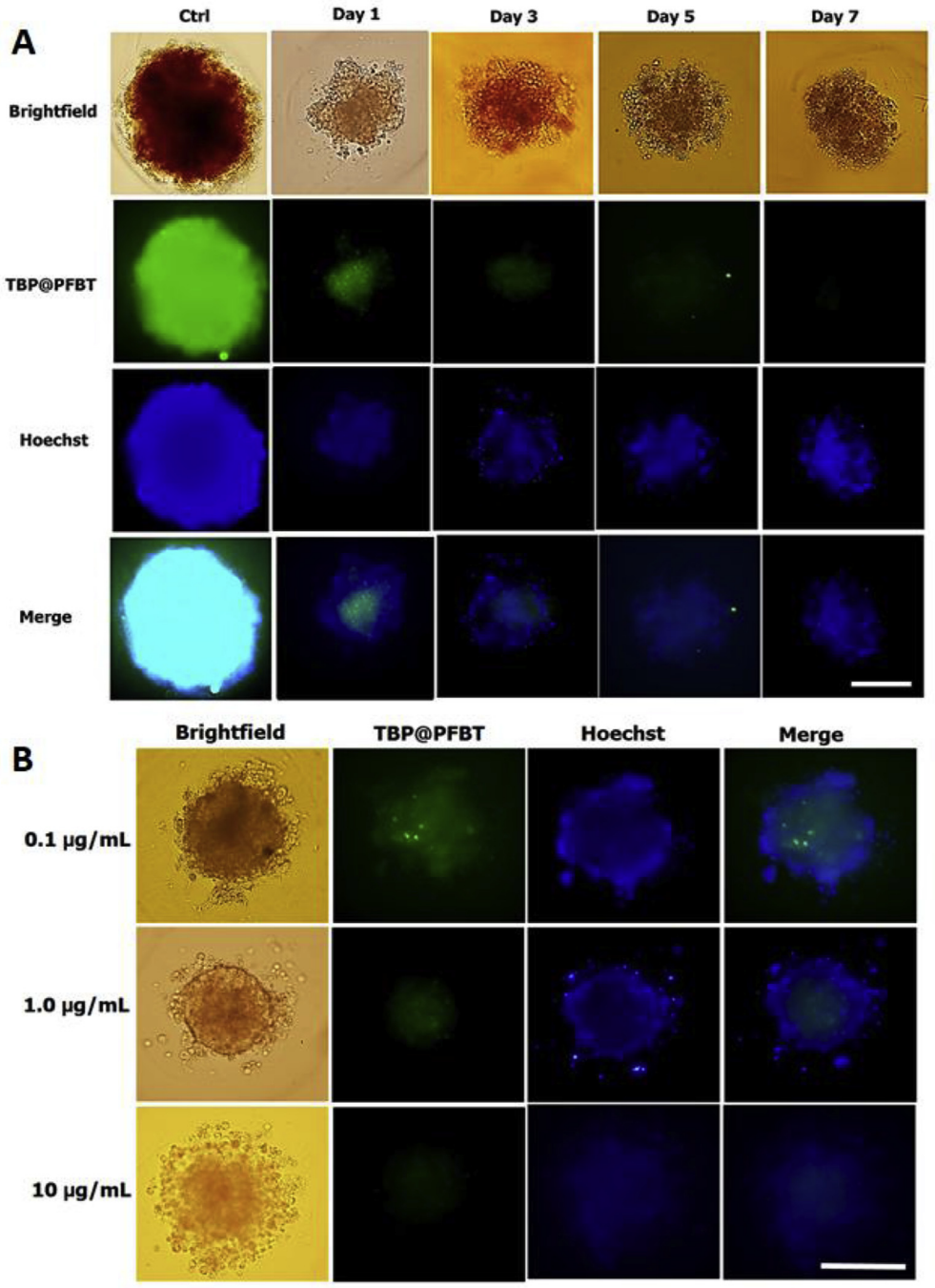

Fig. 5. (A) Qualitative assessment of 10 µgmL^{-1} DOX penetration into tumor spheroids from MCF-7 cells after 2 h incubation of each treatment with TBP@PFBT probe. Scale bars: 100 µm.(B) Qualitative assessment of DOX concentration on MCF-7 tumor spheroids formed at day 3, after 2 h incubation of each treatment with TBP@PFBT probe. Scale bars: 100 µm.

On the contrary, only intense fluorescence emission could be seen for HFF cells within the same period of treatment time (after 24 h) compared to the cells incubated with DOX (Fig. S4). Yellow fluorescence signals inside both cells for different incubation times showed efficient uptake of DOX. The reason for these observations may be due to high storage of iron in cancer cells (i.e., MCF-7) relative to normal cells (i.e., HFF), which released during the apoptotic cell death (Akbari-Birgani et al., 2014; Verdom et al., 2018). In the next step, the probe was applied to the determination of Cyt c in MCF-7 and HFF cells upon excitation at 540 nm for cell lysis after different incubation times (CTLR, 6, 12, 24 h) with DOX, using the fluorescence intensity originating from 100 × 10^3 cells. As it is seen from Table S4, MCF-7 released Cyt c (µM per 100 × 103 cells) rather than HFF cells and maximum concentration of the Cyt c was obtained after 12 h incubation, and was estimated as ~ 0.58 and 0.18 µM for MCF-7 and HFF cells, respectively (Table S4). These results clearly demonstrated that TBP@PFBT not only has potential for a very effective bioimaging but also can be used for specific real-time monitoring of Cyt c and iron ions in early-stage apoptosis allowing cancer cell apoptosis imaging without targeting of the PDs, or any additional reagents according to the performed process (Fig. 4).

The apoptosis induction was also well demonstrated in 3D tumor models. Tumor spheroid systems are used as a 3D vitro model for tumor biology study in cancer research. In Comparison to 2D cell cultures, the

main advantage of tumor spheroid models is the more in vivo-like behavior of the tumor cells resembling animal models. Tumor spheroid models are characterized by the initial phase of cell proliferation followed by a decrease in the percentage of S phase cells and the proliferation gradient formation which decreases from periphery to center. Thereafter, an outer zone of proliferating cells can be distinguished from of inner zone of non-proliferating cells (in the G0-phase). The decline in the population of the cells in the S and G2 phases can result in the reduction of cell growth and proliferation rate which is the representative of early apoptosis in spheroids (Jamali et al., 2018; Seyfoori et al., 2018). Regarding our study, we were supposed to induce apoptosis in the spheroids using DOX in diffident time intervals. After TBP@PFBT applying to the spheroids, the fluorescence quenching was observed and hence, it is revealed that the mechanism of apoptosis induction in the developed tumor spheroid is the same as monolayer tumor cells, through which Cyt c is released into cytoplasm followed by mitochondria membrane lysis. Using this experiment, the capability of the novel fluorescence probe was further confirmed.

As illustrated in Fig. 5A, by applying 10 μgmL^{-1} DOX solution to the spheroid culture media, fluorescent intensity decrement is obvious so that it is an indication of apoptosis progression in the tumor spheroids. However, fluorescent quenching capability of the control untreated spheroids is obviously less than intervened samples, showing the lower amount of released Cyt c in the cytoplasm of the normal spheroids. Moreover, by progress of time, the cell mitochondria are getting more permeable and, hence, the concentration of Cyt c is increased. In addition to investigating the effect of DOX incubation time, various concentrations of the DOX from 0.1 to 10 μgmL^{-1}were also assessed, in orderto clarify the optimum drug concentration in which the apoptosis is more significant. As it is seen from Fig. 5B, the number of cells having fluorescence emission is decreased with increasing DOX concentration so that it seems that a 10 μgmL^{-1} DOX can effectively induce apoptosis in MCF7 spheroids as 3D tumor models.

4. Conclusions

In conclusion, this article describes the preparation and characterization of novel phosphate functionalized semiconducting polymer dots with high brightness, photostability and excellent cellular permeability. By using the prepared PDs, we developed a very high sensitive system for Fe^{3+} ion detection based on aggregation induced fluorescence off mechanism. Very high sensitivity of the probe provided the opportunity to reduce the matrix effect dramatically. Using this approach, we obtained sharp specific apoptosis imaging in early stage breast cancer cells, together with effective sensing of Fe(III) ion and Cyt c in environmental samples and in cell lysates, respectively, with detection volumes of less than 10 μL and without any noticeable interference from matrix constituents. In this study Cyt c as an indication of early apoptosis was detected through fluorescent intensity quenching in both monolayer and spheroid developed breast tumor models so that after DOX applyication a significant intensity alteration was monitored within the whole monolayer cells or spheroids, compared to the control sample. This simple, sensitive, and economicaltechnique takes the advantage of high brightness and opticaltune-ability of semiconducting polymer nanoparticles and affordsa means of rapid determination of Fe^{3+} ion in biologicalor environmental samples. This probe is also applicable for copper measurement in places that iron ions are not present. Compared to other fluorescence probes for detection of Fe^{3+} ions and Cyt c, it was found that the synthesis process for TBP@PFBT PDS is one-step, fast and very friendly. Importantly, this label-free assay provides short determination time of only a few min, easy operation, and much lower LOD, allowing 100–4000 times increase in sensitivity over previously reported probes, as well as high specificity without need to using biorecognition elements such as enzymes, antibodies and/or aptamers while its excellent features made the TBP@PFBT PDs a highly efficient probe for successful apoptosis imaging in live cells.

Declaration of interests

The authors declare that they have no known competing financial interests or personal relationships that could have appeared to influence the work reported in this paper.

CRediT authorship contribution statement

Ammar Chabok: Investigation, Formal analysis, Formal analysis. **Fatemeh Molaabasi:** Conceptualization, Validation, Writing - review & editing. **Amir Seyfoori:** Methodology, Data curation. **Behnam Hajipour-Verdom:** Formal analysis. **Behnaz Shojaedin-Givi:** Investigation, Formal analysis. **Mosslim Sedghi:** Project administration, Supervision, Writing - review & editing, Software. **Hosein Naderi-Manesh:** Validation, Visualization. **Ali Yeganeh-Faal:** Resources, Funding acquisition.

Acknowledgements

The financial support of this work by Iran Science Elites Federation (ISEF) and Research Councils of Tarbiat Modares and Razi Universities is gratefully acknowledged. We also thank Payam Noor University, Qom Branch, for the laboratory support.

Appendix A. Supplementary data

Supplementary data to this article can be found online at https://doi.org/10.1016/j.bios.2019.111337.

References

Akbari-Birgani, S., Hosseinkhani, S., Mollamohamadi, S., Baharvand, H., 2014. J. Biol. Chem. 289, 16905–16913.
Bartl, H., Kuppers, H., 1980. ZeitschriftfürKristallographie 152, 161–167.
Benedict, M., Bigford, T.H., Levi, H.W., 1981. Nuclear Chemical Engineering, 2th ed. McGraw Hill.
Chabok, A., Shamsipur, M., Yeganeh-Faal, A., Molaabasi, F., Molaei, K., Sarparast, M., 2019. Talanta 194. pp. 752–762.
Chan, Y.H., Jin, Y., Wu, C., Chiu, D.T., 2011. Chem. Commun. (J. Chem. Soc. Sect. D) 47, 2820–2822.
Childress, E.S., Roberts, C.A., Sherwood, D.Y., LeGuyader, C.L.M., Harbron, E.J., 2012. Anal. Chem. 84 (3), 1235–1239.
Fabry, L., Pahlke, S., Kotz, L., Tolg, G., 1994. Fresenius. J. Anal. Chem. 349 (4), 260–271.
Feng, L., Zhu, C., Yuan, H., Liu, L., Lv, F., Wang, S., 2013. Chem. Soc. Rev. 42, 6620–6633.
Georgopoulos, P.,G., Roy, A., Yonone-Lioy, M.,J., Opiekun, R.E., Lioy, P.J., 2001. J. Toxicol. Environ. Health, Part B 4, 341–394.
Hsu, K.,W., Huang, C.,Y., Tam, K.,W., Lin, C.,Y., Huang, L.,C., Lin, C.,L., Hsieh, W.,S., Chi, W.,M., Chang, Y.,J., Wei, P.,L., Chen, S.,T., Lee, C.,H., 2018. Int. J. Mol. Sci. 19, 452.
Huang, C.,C., Yang, Z., Lee, K.,H., Chang, H.,T., 2007. AngewandteChemie. International Edition46, pp. 6824–6828.
Hudson, R.J., Covault, D.T., Morel, F.M., 1992. Mar. Chem. 38 (3–4), 209–235.
Irving, H., Edgington, D., 1959. J. Inorg. Nucl. Chem. 10 (3–4), 306–318.
Jamali, T., Kavoosi, G., Safavi, M., Ardestani, S.K., 2018. Sci. Rep. 8 (1), 15787.
Kozlowski, H., Brown, D.R., Valensin, G., 2006. Metallochemistry of Neurodegeneration. RSC Publishing, Cambridge, UK.
Li, Q., Zhang, J., Sun, W., Yu, J., Wu, C., Qin, W., Chiu, D.T., 2014. Langmuir 30, 8607–8614.
Meng, Q., Zhang, X., He, C., He, G., Zhou, P., Duan, C., 2010. Adv. Funct. Mater. 20, 1903–1909.
Nasirian, V., A, Chabok, A., Barati, M., Rafienia, M., Sheikh Arabi, M., Shamsipur, M., 2017. Microchimica Acta 184, 4655–4662.
Ruan, L., Xu, Z., Lan, T., Wang, J., Liu, H., Li, C., Dong, C., Ren, J., 2012. Anal. Chem. 84, 7350–7358.
Ryan, K.J., Ray, C.G. (Eds.), 2004. Sherris Medical Microbiology, fourth ed. McGraw Hill, N.Y, pp. 624–628.
Seyfoori, A., Samiei, E., Godau, B., Jalili, N., Farahmand, L., Majidzadeh, K., Akbari, M., 2018. Lab Chip 18, 3516–3528.
Shamsipur, M., Molaabasi, F., Hosseinkhani, S., Rahmati, F., 2016. Anal. Chem. 88, 2188–2197.
Smolin, F.O., Mitra, R., Thiele, M., Daniliuc, C.G., Stegemann, L., Strassert, C., Niemeyer, J., 2017. Chem. Eur J. 23 (42), 10058–10067.
Song, J.M., Kasili, P.M., Griffin, G.D., Vo-Dinh, T., 2004. Anal. Chem. 76, 2591–2594.
Subarkhan, M., Kasim, M., Sundar, S., Rengan, R., 2018. Inorgan. Chem. Front. 5, 585–596.
Sun, I.C., Lee, S., Koo, H., Kwon, I.C., Choi, K., Ahn, C.H., Kim, K., 2010. Bioconjug.

Chem. 21, 1939–1942.
Sun, W., Ye, F., Gallina, M.E., Yu, J., Wu, C., Chiu, D.T., 2013. Anal. Chem. 85, 4316–4320.
Sunda, W., Huntsman, S., 2003. Mar. Chem. 84 (1–2), 35–47.
Tong, F., Lian, Y., Zhou, H., Shi, X., He, F., 2014. Anal. Chem. 86 (20), 10415–10421.
Torkzadeh-Mahani, M., Ataei, F., Nikkhah, M., Hosseinkhani, S., 2012. Biosens. Bioelectron. 38, 362–368.
Torrado, A., Walkup, G.K., Imperiali, B., 1998. J. Am. Chem. Soc. 120, 609–610.
Verdom, B.H., Abdolmaleki, P., Behmanesh, M., 2018. Scientific Reports8. pp. 990–1001.
Waterhouse, N., Trapani, J., 2003. Cell Death Differ. 10, 853–855.
Wen, Q., Zhang, X., Cai, J., Yang, P.-H., 2014. Analyst 139, 2499–2506.
Wu, C., Chiu, D.T., 2013. Angewandte Chemie 52 (11), 3086–3109 International Edition.
Wu, C., Bull, B., Szymanski, C., Christensen, K., McNeill, J., 2008a. ACS Nano 2 (11), 2415–2423.
Wu, C., Zheng, Y., Szymanski, C., McNeil, J., 2008b. J. Phys. Chem. C 112, 1772–1781.
Wu, C., Schneider, T., Zeigler, M., Yu, J., Schiro, P.G., Burnham, D.R., McNeill, J.D., Chiu, D.T., 2010. J. Am. Chem. Soc. 132, 15410–15417.
Wu, C., Hansen, S.J., Hou, Q., Yu, J., Zeigler, M., Jin, Y., Burnham, D.R., McNeill, J.D., Olson, J.M., Chiu, D.T., 2011. Angew. Chem. Int. Ed. 50 (15), 3430–3434.
Wu, Y., Zhou, H., Wei, W., Hua, X., Wang, L., Zhou, Z., Liu, S., 2012. Anal. Chem. 84, 1894–1899.
Wu, P.J., Kuo, S.Y., Huang, Y.C., Chen, C.P., Chan, Y.H., 2014. Anal. Chem. 86, 4831–4839.
Zhang, S., Zhu, S., Yang, L., Zheng, Y., Gao, M., Wang, S., Zeng, J.Z., Yan, X., 2012. Anal. Chem. 84, 6421–6428.
Zhang, Y., Wang, G., Zhang, J., 2014. Sensor. Actuator. B 200, 259–268.